Earth Planet. Sci. Lett. 690 (2026) 120133

Contents lists available at ScienceDirect

Earth and Planetary Science Letters

journal homepage: www.elsevier.com/locate/epsl

Garnet pyroxenite at mid-mantle depths as a source of young lunar magmatism

Dian Ji *, Rajdeep Dasgupta

Department of Earth, Environmental and Planetary Sciences, Rice University, 6100 Main Street, MS 126, Houston, TX 77005, USA

ARTICLE INFO

Edited By: Dr Fang-Zhen Teng

Keywords:
The Moon
Chang'e-5
Young lunar magmatism
Garnet
Mantle melting
Mantle overturn

ABSTRACT

As the youngest returned mare basalt to date, deciphering the petrogenesis of Chang'e-5 (CE-5) basalts could assist us in understanding the late-stage lunar mantle evolution. However, the lithology of the CE-5 mantle is still controversial. Here, we present a joint study of high pressure-temperature major element phase equilibria using laboratory experiments and trace element modeling, and show that garnet is present in the source of young mare basalts on the Moon. Our high-pressure-temperature experiments approaching the multiple saturation point of the putative parental melt compositions of young CE-5 basalt show garnet and clinopyroxene coexisting with the quenched silicate melt. Trace element modeling also confirms that small amounts of garnet in the mantle source are required to reconcile the rare-earth element pattern of the CE-5 basalts, regardless of whether the CE-5 basalts were the direct mantle-melting products or produced through extensive fractional crystallization of a primitive basalt. The existence of garnet in the source either implies that lunar mantle overturn played a crucial role in contributing to the lunar mantle heterogeneity, creating a garnet-clinopyroxenitic mantle source of these young mare basalts that survived the subsequent mantle evolution, or a late-stage process introduced fertile material into the deep mantle, and such geodynamic processes within the lunar interior may have continued until 2 Ga.

1. Introduction

The mineralogical assemblage that participates in the partial melting of rocky planetary mantles provides insight into the composition, thermal structure, dynamics, and pressure-temperature (*P-T*) conditions of the planetary interior. For rocky bodies that remain magmatically and volcanically active over a long period, the crustal magmatic products can provide clues on the temporal evolution of the mineralogic make-up of the mantle domain. Such a temporal record of the source lithology and the associated conditions of mantle melting of rocky planetary interiors is mostly restricted to Earth (e.g., Herzberg et al., 2010), with some constraints derived by combining meteorite data and surface chemistry also for Mars (e.g., Filiberto and Dasgupta, 2011, 2015). Recently completed Chang'e-5 (CE-5) mission on the Moon brought back lunar mare basalts only ~2 Ga old (Che et al., 2021; Li et al., 2021). This provides a unique opportunity to probe evolution of another planetary mantle, i.e., that of the lunar mantle, over >2 billion years. However, geochemical investigation of the CE-5 data, probing the interior of the young Moon, remains far from complete.

The young CE-5 basalts show low MgO, and high FeO* contents (Fig. 1), representing relatively evolved lunar melts (Chen et al., 2023). In particular, they exhibit concentrated trace element abundances, with relative enrichment in light rare earth elements (REEs) compared with heavy REEs and obvious negative Eu anomalies (Wu et al., 2024). Such signatures are commonly attributed to mineral fractionation, or the presence of residual phases during mantle melting (e.g., plagioclase, clinopyroxene, and garnet; Castillo, 2012), and/or the magma mixture/contamination with a light REE enriched component with negative Eu anomaly [e.g., KREEP (K, rare Earth element, and P-rich) component; (Warren and Wasson, 1979)]. Utilizing trace element modeling and isotopic characteristics, the study by Tian et al. (2021) proposed that the CE-5 basalts are generated by extensive fractional crystallization after low-degree mantle melting. This suggestion was supported and further developed by several major and trace element modeling studies (He et al., 2022; Yang et al., 2022), suggesting a deep mantle (~500 km; Su et al., 2022) with mixed lithology consisting of early and late lunar magma ocean (LMO) cumulates would be required to lower the melting point of the source (Su et al., 2022) and satisfy the stable isotope

* Corresponding author.
E-mail address: dj56@rice.edu (D. Ji).

https://doi.org/10.1016/j.epsl.2026.120133
Received 28 January 2026; Received in revised form 21 April 2026; Accepted 21 May 2026

characteristics (Jiang et al., 2023). In addition, a small amount of KREEP component was suggested to be necessary, thereby explaining the incompatible elements of CE-5 soil and basaltic clasts, as well as isotopic characteristics of the mantle source (Wang et al., 2024c; Zong et al., 2022). Although the fractional crystallization of the CE-5 primitive melt is necessary for reproducing a series of more evolved CE-5 basaltic clasts (Tian et al., 2021; Su et al., 2022; Hoyos and Grove, 2023), Haupt et al. (2023) cast doubt on the necessity of extensive fractional crystallization to reproduce the CE-5 primitive melt, since the lunar mantle is heterogenous and could be locally enriched in FeO (Elardo et al., 2025). Accordingly, Haupt et al. (2023) suggested that the most primitive CE-5 basalt can be reproduced by direct partial melting of a shallow, clinopyroxene-dominant source (~250 km) based on high *P-T* experiments. This idea is also supported by elemental modeling of CE-5 whole rock and minerals (Luo et al., 2023; Wang et al., 2024a), indicating that the most primitive CE-5 basalt can be generated by partial melting of the lunar pyroxenitic mantle with minor olivine and oxides.

A key question related to CE-5 mare basalt genesis is what allowed lunar magmatism to continue late. Late magmatism in a small planetary body requires either an easily fusible mantle domain to persist or a heat source that could induce partial melting. Contrasting ideas have emerged on this question. Recently, Elardo et al. (2025) proposed the parental melt of young CE-5 basalts is generated by the partial melting of a shallow plagioclase-bearing pyroxenitic mantle, and that the KREEP layer at the crust-mantle boundary acted as the top-down heat source to maintain the lunar magmatism until ~2 Gyrs ago. This hypothesis was challenged more recently by the modeling study of Li et al. (2025), where the authors argued these youngest mare basalts were derived from a plagioclase-free lunar lower mantle, and garnet was required in the source region in order to reconcile the rare earth element pattern of the primitive melt. The hypothesis that the young lunar mantle contains garnet is consistent with the earlier study by Yang et al. (2022) that argued for source garnet to reconcile the geochemical characteristics of the CE-5 impact glass beads. Moreover, Li et al. (2025) argued for a partially molten layer near the core-mantle boundary to be the source of CE-5 basalts.

With very few exceptions (e.g., Haupt et al., 2023; Elardo et al., 2025), almost all previous works highly relied on thermodynamic modeling to constrain the source lithology of CE-5 mare basalt and mantle melting *P-T* conditions. Thermodynamic models exhibit varying degrees of discrepancy when applied to compositions of lunar basalts and the corresponding oxygen fugacities compared to results of high *P-T* experiments (e.g., Astudillo Manosalva and Elardo, 2024; Ji and Dasgupta, 2025). These discrepancies vary across thermodynamic models and are difficult to quantify and correct accordingly. In addition, the only two experimental studies employed parental melt compositions that were relatively similar (Fig. 1), and focused only on relatively low-pressure conditions (<1.8 GPa; Elardo et al., 2025; Haupt et al., 2023). To our knowledge, no experimental studies covered *P-T* conditions where CE-5 mare basalts could originate from a primitive source and/or deep lunar mantle (e.g., Su et al., 2022; Li et al., 2025).

In order to constrain the mantle lithology of the CE-5 mare basalts

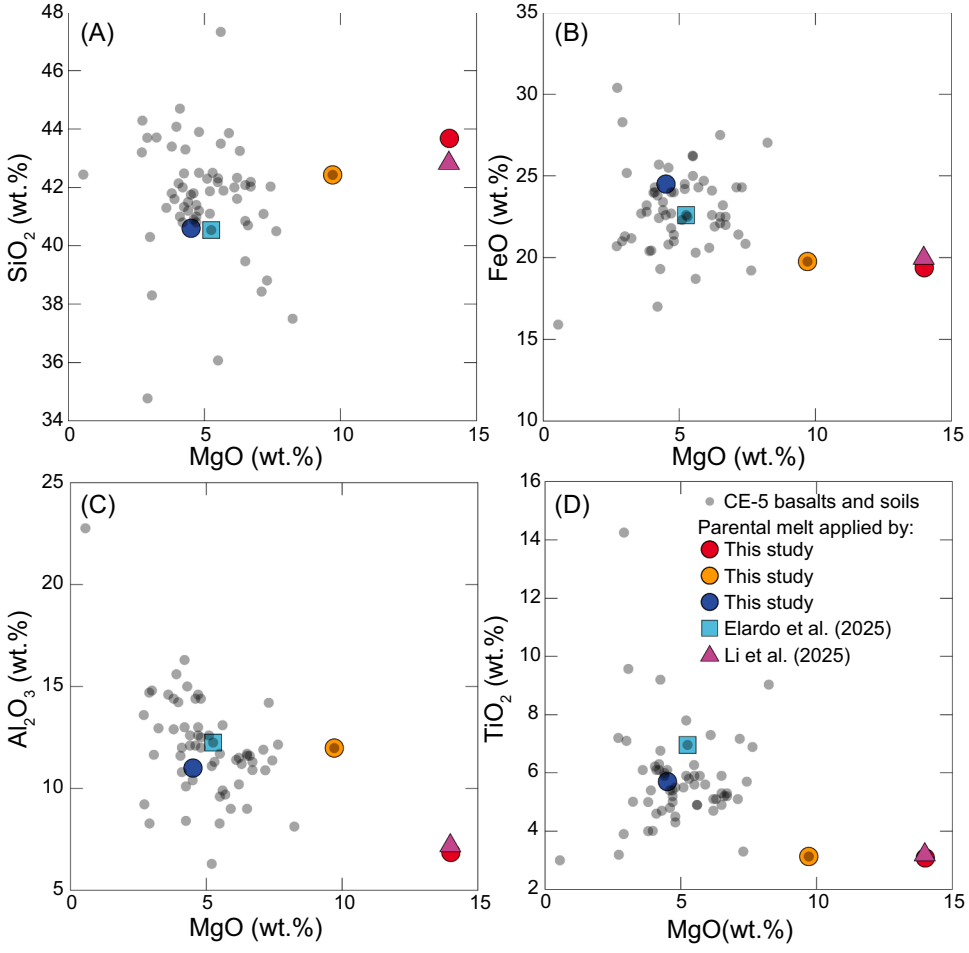

Fig. 1. The major element compositions of putative CE-5 parental melts applied in this study, and the studies of Elardo et al. (2025) and Li et al. (2025). The red circle represents composition from Su et al. (2022), while the orange and blue circles represent composition from Luo et al. (2023) and Haupt et al. (2023), respectively. Also plotted are whole rock compositions of CE-5 basalts and soils as small grey circles for comparison (Che et al., 2021; Jiang et al., 2023; Su et al., 2022; Tian et al., 2021; Wang et al., 2024c; Zong et al., 2022).

from a more comprehensive perspective considering different parental melt compositions, and therefore to better understand the late-stage physical evolution of the lunar mantle, in this study we combined high *P-T* experiments, trace element modeling, and the existing isotopic evidence to constrain the origin of the CE-5 basalts. We specifically aimed to constrain the source lithology and the conditions of mantle melting, focusing on the primitive melt prior to the possible onset of fractional crystallization. Our combined approach provided several lines of evidence for the presence of garnet in the young lunar mantle. We further applied our method to Apollo 12 low-Ti basalt and discussed the implications of our findings in the light of lunar mantle evolution and dynamics.

2. Phase equilibria experiments

Traditionally, two experimental strategies are used to assess the source mantle lithology of a primitive silicate melt of terrestrial planets. Both strategies have been applied on the Moon. The "forward" approach involves melting a model mixture based on an assumed mantle source, and comparison of the generated melts with estimated compositions of primitive surface basalts to provide insight on the source lithology or further components that may be required (e.g., Moitra et al., 2026; Singletary and Grove, 2008). Conversely, the "inverse" approach uses the putative parental melt as the starting composition to experimentally determine conditions where that melt may be multiply saturated with expected mantle minerals, revealing the residual mantle lithology the parental melt was last in equilibrium with (e.g., Green et al., 1975; Krawczynski and Grove, 2012). For the CE-5 basalt, the forward approach is challenging, because no direct mantle samples are available for the Moon and the highly debated parental melt composition leads to widely varying estimates of source lithology. Therefore, many different iterations of direct partial melting experiments could be needed. Furthermore, the young lunar mantle likely experienced deviation from primary magma ocean crystallization products due to lunar mantle overturn, the extent of which is also a matter of debate. Consequently, we utilize the inverse multiple saturation approach to circumvent these uncertainties.

2.1. Starting materials

The experimental starting materials were the CE-5 parental melt compositions recommended by Su et al. (2022), Luo et al. (2023), and Haupt et al. (2023) (Fig. 1; Table S1). The parental melt composition proposed by Su et al. (2022) is relatively primitive (Mg# = 56; Fig. 1), as the authors believe that after mantle melting, the CE-5 parental melt experienced extensive fractional crystallization. This melt is close to the one applied by Li et al. (2025). The parental melt proposed by Luo et al. (2023) is the CE-5 clast with the highest Mg# (Mg# = 47) and lowest TiO_2 concentration (3.13 wt.%; Fig. 1) among all CE-5 basalts and soils. The composition applied in Haupt et al. (2023) is from Che et al. (2021) and is highly evolved (Mg# = 25; Fig. 1), which may not appear to represent a primary melt from the CE-5 mantle. However, Elardo et al. (2025) applied the olivine-melt Fe-Mg exchange coefficients to examine a series of CE-5 basaltic clasts and believed the clast 103–001, 005 from Tian et al. (2021) is most suitable as the parental melt, with the major element compositions that are very similar to those utilized by Haupt et al. (2023) (compare blue circle and cyan square in Fig. 1). For this reason, we still utilize the composition from Haupt et al. (2023) as a potential parental melt composition.

2.2. High P-T experiments

We conducted 28 high *P-T* experiments at the Experimental Petrology Laboratory of Rice University using an end-loaded piston-cylinder (PC: 1.5–3.0 GPa) and a Walker-style multi-anvil (MA: 3.0–5.0 GPa) device at 1.5–5.0 GPa and 1250–1600 °C, following the pressure-temperature calibration and procedure reported in Tsuno and Dasgupta (2011) and Ding et al. (2014), and adopted in many subsequent terrestrial and lunar studies (e.g., Carter and Dasgupta, 2015, Tsuno and Dasgupta, 2015; Ding et al., 2018; Pal and Dasgupta, 2024). We also combine an additional 9 experiments conducted and reported by Ji and Dasgupta (2025), which added FeS in the starting materials. Barring two experiments at lower pressure (1.5 GPa; B669 and B675), which applied single graphite capsules, all other experiments utilized Pt capsules with graphite inner (Fig. 2A), in order to prevent the ingress of water during the experiment, yet preventing Fe-loss to Pt (Table S2). All experimental procedures are detailed in the Supplementary Material.

2.3. Analysis

Major element concentrations of the experimental phases and the texture of the experimental products were investigated using a JEOL JXA-8530F Hyperprobe at Rice University and a Shimadzu 8050 G Electron Probe Microanalyzer at the University of Texas, Austin. WDS spot analyses were performed using natural and synthetic standards (see Supplementary Material for details).

3. Evidence of garnet in the source of CE-5 basalts from experiments

The phase assemblages and estimated phase proportions as a function of *P-T* conditions of experiments for three putative CE-5 parental melts are listed in Table 1. Detailed description and compositions of experimental products are provided in the supplementary materials and Table S2.

For experiments with the initial composition from Su et al. (2022), clinopyroxene is the only liquidus phase at 3.0 to 4.0 GPa, 1500 to 1550 °C. Garnet only enters the phase assemblage at temperatures <1500 °C at 2.5 GPa, and 1550 °C at 4.0 GPa, while garnet and clinopyroxene both exist as liquidus phases at pressures of 4.5 GPa and 5.0 GPa (Fig. 3). When applying LS0–1 (Luo et al., 2023; Table S1) as the starting melt, clinopyroxene is the liquidus phase until the experimental pressure approaches 2.0 GPa, at which point garnet becomes the sole liquidus phase. With increasing pressures, the experiments with HS0–1 (Haupt et al., 2023; Table S1) start producing garnet and clinopyroxene as the liquidus phases at ~1.5 GPa, 1300 °C, while garnet is the only liquidus phase at the pressure of 2.0 GPa. After accounting for measurement uncertainties, the melt in equilibrium with garnet at the conditions near the liquidus exhibits major element compositions nearly identical to those of the starting mix (e.g., MA350, G866, and G869; Fig. 2; Table S2). The experiments approached equilibrium with respect to major and minor element exchanges and partitioning (Fig. S1; see supplementary materials for more discussion).

Based on experimental results in this study and those in Ji and Dasgupta (2025), we constructed *P-T* diagrams showing the phase assemblage regarding CE-5 parental melt. All three initial components exhibit two MSPs, with garnet and clinopyroxene being the liquidus minerals at the higher *P-T* MSP (Fig. 3), suggesting these two minerals may define the source mineralogy of CE-5 parental melt. The garnet-free MSP for the more primitive parental melt composition SS0–2 is at ~1.7 GPa, 1475 °C, and garnet-present MSP is at ~4.75 GPa, 1580 °C (Fig. 3B). As HS0–1 and LS0–1 represent more evolved parental melt (Fig. 1), the MSPs with garnet are shallower than that for SS0–2, i.e., they are at ~1.75 GPa, 1375 °C and ~1.75 GPa, 1450 °C respectively. Garnet-free MSPs also appear for these two compositions, at ~1.25 GPa-1300 °C and ~1.00 GPa-1320 °C, where clinopyroxene and spinel are the liquidus phases (Fig. 3B).

For phase equilibria studies on CE-5 parental melt, both experimental work by Haupt et al. (2023) and calculations conducted by Su et al. (2022) and Luo et al. (2023), only observed MSPs without garnet as the liquidus phase. Haupt et al. (2023) primarily focused on a relatively low-pressure range (1.0–1.8 GPa). Compared to their work,

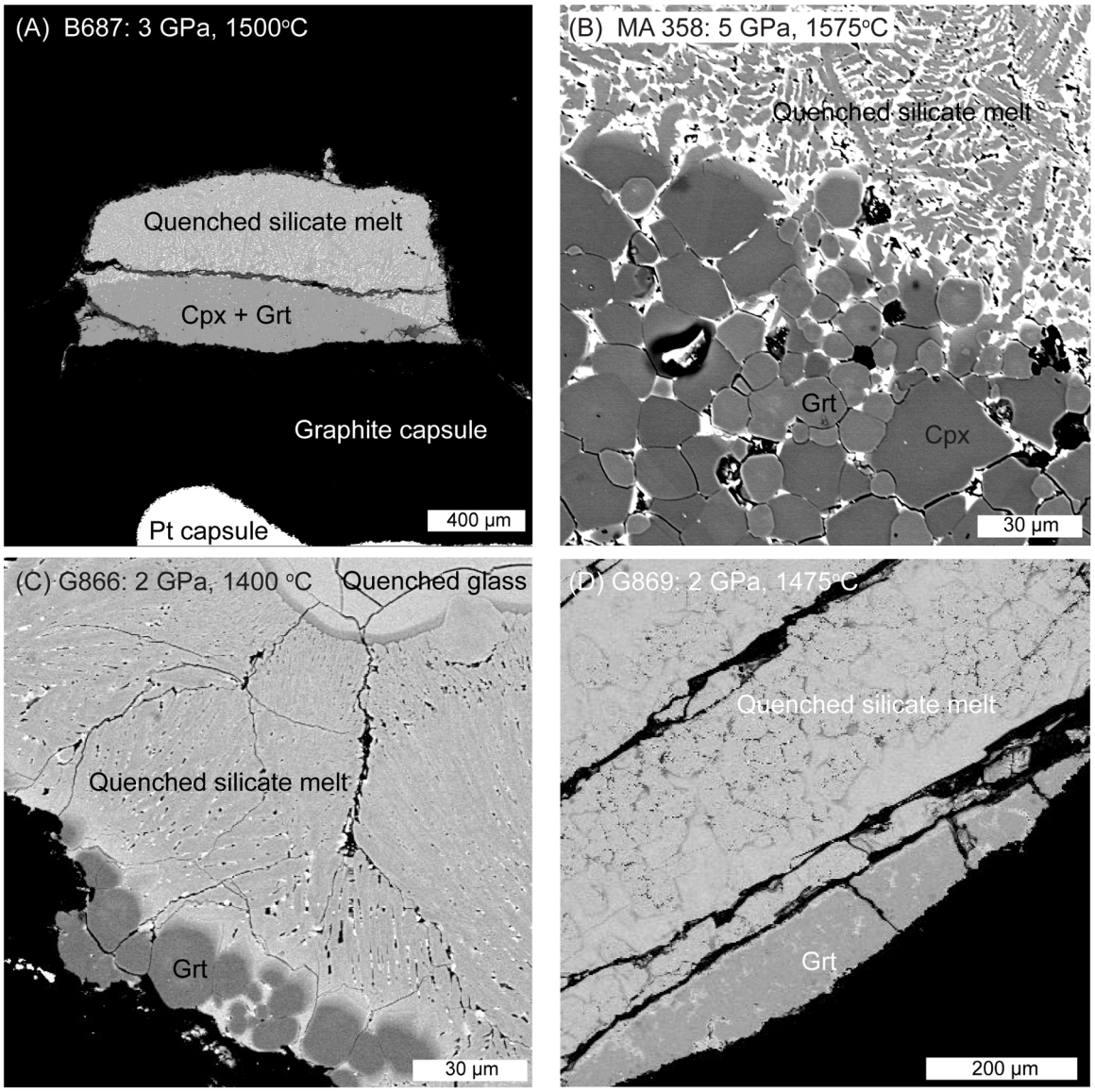

Fig. 2. Representative backscattered electron (BSE) images of our experiments. (A) An overview of experiment B687 (3 GPa, 1500 °C, with starting melt SS0–2) with Pt-graphite double capsule showing segregated melt pool at the top, underlain by residual clinopyroxene (Cpx) and garnet (Grt). (B) Crystallized minerals containing clinopyroxene and garnet in the multi-anvil experiment MA358, at 5 GPa and 1575 °C, with starting melt SS0–2. (C-D) Experiments G866 (2 GPa, 1400 °C, with starting melt HS0–1) and G869 (2 GPa, 1475 °C, with starting melt LS0–1) with garnet as the only crystallized mineral.

our experiments indicated a garnet-free MSP that is ~50 °C higher than their prediction (~1.3 GPa, 1225 °C). Moreover, no garnet was reported in their experiments at 1.5 and 1.8 GPa. These differences may be related to the experimental assembly employed by Haupt et al. (2023). They utilized a hydrous talc sleeve with the graphite-only capsule, which may introduce weight percent-level water into their experiment by dehydration of the talc (Elardo et al., 2025; McCubbin et al., 2015), thereby lowering the MSP and altering the phase assemblage. Our experiments with starting melt SS0–2, compared with the THERMOCALC modeling in Su et al. (2022), suggested the garnet-free MSP that is ~0.5 GPa lower in pressure and ~25 °C higher in temperature than those predicted by thermodynamic modeling. In addition, unlike the prediction from THERMOCALC, no orthopyroxene was observed as the liquidus phase in our phase equilibrium experiments. The pMELTS modeling in Luo et al. (2023) focuses only on the relatively low-pressure range (up to 1.5 GPa), and the crystallized phases in the experiment at 1 GPa largely corresponded with the pMELTS modeling, while the pMELTS failed to predict the crystallization of garnet at 1.5 GPa, 1300 °C. These differences again demonstrate the deviation between thermodynamic modeling and experiments for lunar-relevant compositions, emphasizing the importance of high *P-T* experiments in constraining the potential lunar mantle lithology and mantle melting conditions.

4. Evidence of garnet in the lunar mantle from trace element modeling

4.1. Model setup

Trace element modeling was conducted to investigate whether the phase assemblages suggested by high *P-T* experiments can reproduce the trace element characteristics of CE-5 basalt for different proposed petrogenesis of three parental melt compositions investigated in this study. For trace element modeling, we mainly focus on rare-earth elements (REEs). We primarily used the average composition of CE-5 scooped soil (Zong et al., 2022) to represent the REE pattern of the CE-5 parental melt and further used average compositions of drilled soil and basaltic clasts (Jiang et al., 2023; Wang et al., 2024b) to verify our modeling results. In tracking the trace element fractionation, we did not

Table 1
Experimental conditions and products.

Sample	*P* (GPa)	*T* (°C)	Duration (h)	Starting material	Calculated phase proportion	R^{2} [c]
MA361	5	1600	3	SS0–2	Melt (100)	-
MA358	5	1575	5	SS0–2	Cpx (27), Grt (15), Melt (58)	0.999
MA355	4.5	1575	3.5	SS0–2	Melt (100)	-
MA357	4.5	1550	5	SS0–2	Cpx (25), Grt (4), Melt (71)	0.999
MA341	4	1650	1.5	SS0–2	Melt (100)	-
MA350	4	1550	6.5	SS0–2	Cpx (4), Melt (94)	1.000
MA353	4	1500	16.5	SS0–2	Cpx (33), Grt (8), Melt (58)	0.999
MA337	3.5	1650	2	SS0–2	Melt (100)	-
MA352	3.5	1525	11.5	SS0–2	Cpx (8), Melt (92)	1.000
MA354	3.5	1475	12	SS0–2	Cpx (12), Melt (88)	0.999
G894	3	1550	21	SS0–2	Melt (100)	-
MA343	3	1550	2	SS0–2	Melt (100)	-
MA349	3	1500	17	SS0–2	Cpx (15), Melt (86)	1.000
B687[a]	3	1500	22	SS0–2	Cpx (29), Grt (0), Melt (71)	1.000
G896	2.5	1550	17.5	SS0–2	Melt (100)	-
B619[b]	2.5	1500	18	80 wt.% SS0-2 + 20 wt.% FeS	Cpx (19), Melt (83)	0.998
B688	2.5	1450	24.5	SS0–2	Cpx (45), Grt (1), Ol (0), Melt (56)	1.000
B670[b]	2	1550	5	80 wt.% SS0-2 + 20 wt.% FeS	Melt (100)	-
B629[b]	2	1500	8	80 wt.% SS0-2 + 20 wt.% FeS	Cpx (3), Melt (97)	1.000
B671[b]	1.5	1500	15	80 wt.% SS0-2 + 20 wt.% FeS	Melt (100)	-
G895	2.5	1525	22	LS0–1	Melt (100)	-
G893	2.5	1475	21	LS0–1	Cpx (10), Grt (11), Melt (79)	1.000
G885	2	1500	18	LS0–1	Melt (100)	-
G869	2	1475	19	LS0–1	Grt (0), Melt (100)	1.000
B750	2	1400	25	LS0–1	Cpx (21), Grt (12), Melt (66)	1.000
G871	1.5	1400	23.5	LS0–1	Melt (100)	-
B665[b]	1.5	1350	20	80 wt% LS0-1 + 20 wt% FeS	Cpx (10), Melt (91)	1.000
B675	1.5	1300	68	LS0–1	Cpx (35), Grt (10), Melt (55)	1.000
B649[b]	1	1350	23	80 wt% LS0-1 + 20 wt% FeS	Melt (100)	-
B708[b]	1	1300	53	80 wt% LS0-1 + 20 wt% FeS	Cpx (11), Sp (1), Melt (89)	0.999
G870	2	1450	24.5	HS0–1	Melt (100)	-
G866	2	1400	24	HS0–1	Grt (0), Melt (100)	1.000
G874	1.5	1350	47	HS0–1	Melt (100)	-
G872	1.5	1300	48	HS0–1	Cpx (19), Grt (11), Melt (70)	1.000
B669	1.5	1250	68	HS0–1	Cpx (34), Grt (16), Melt (52)	0.997
B667[b]	1.5	1200	72	88 wt.% HS0-1 + 12 wt.% FeS	Cpx (30), Grt (26), Melt (43)	0.995
T312[b]	1	1250	18	98 wt.% HS0-1 + 2 wt.% FeS	Sp (0), Melt (100)	1.000

The table is organized by starting mixes of the runs, and then for a given starting composition, the experiments are arranged in the order of decreasing P and then decreasing T. Ol = olivine, Cpx = clinopyroxene, Grt = garnet, Sp = spinel, Melt = quenched silicate melt.
a. Garnets are very small in size, with only two analyzed spots yielding reliable compositions.
b. The experiments from Ji and Dasgupta (2025) containing FeS in the initial compositions. We did not consider the proportion of FeS in the phase proportion calculation.
c. R^2 is calculated as one minus the ratio of the residual sum of squares to the total sum of squares, representing the fraction of total variance explained by the model. A R^2 value closer to 1 indicates a better fit, meaning the reconstructed compositions closely reproduce the bulk composition, whereas a lower R^2 reflects poorer fitness and larger deviations from the bulk composition.

select mineral-melt partition coefficients from different studies as was done in most of the previous models for CE-5 mare basalts, as partition coefficient is a function of pressure, temperature, compositions, and oxygen fugacity, while failing to consider these factors during mantle melting calculations of different assumed sources could lead to potential bias. Therefore, we applied the experimentally parameterized partition coefficient models between silicate melt and minerals (e.g., Ji and Dygert, 2024; Dygert et al., 2025), as summarized in supplementary materials. To minimize modeling uncertainties and ensure that the calculated results closely approximate mantle melting scenarios under our assumed MSP conditions, we used the *P-T* of the corresponding MSPs (Fig. 2) in the calculations, depending on whether the assumed source contains garnet. We adopted the mineral compositions required in the parameterized models for mantle melting and subsequent fractional crystallization from experiments MA357, G893, and G872, corresponding to parental melt compositions recommended by Su et al. (2022); Luo et al. (2023); and Haupt et al. (2023), respectively. This approach was chosen because these experiments have the *P-T* conditions close to the MSP and contain both garnet and high-Ca pyroxene in the experimental products. The olivine composition was from experiment B688, the only experiment in our study to produce olivine.

4.2. The garnet in the mantle source of young CE-5 mare basalt

We first investigated the petrogenesis model, which posits that the CE-5 basalt was generated by partial melting of a deep mantle source, followed by extensive fractional crystallization (He et al., 2022; Su et al., 2022; Tian et al., 2021; Yang et al., 2022). The assumed REE pattern of the mantle source was a cumulate that corresponds to 86 percent solidification (PCS) of LMO with 2% of trapped liquid (TL) proposed by Tian et al. (2021), and applied in the subsequent studies (Wang et al., 2024c; Zong et al., 2022). This source has a $^{147}Sm/^{144}Nd$ of 0.227, consistent with the required mantle $^{147}Sm/^{144}Nd$ ratio (0.222–0.227; Tian et al., 2021), as determined from the Sm-Nd isotopic data of merrillite from the CE-5 basalts and further verified by Shen et al. (2025). The trace element modeling by Tian et al. (2021) assumed that the mineral mode during mantle melting contains 23% orthopyroxene and 3% plagioclase, in addition to the olivine and high-Ca pyroxenes. Likewise, the major-element modeling using THERMOCALC by Su et al. (2022) indicated that orthopyroxene, rather than clinopyroxene, is the liquidus phase with olivine. However, neither orthopyroxene nor plagioclase was produced in our experiments (Fig. 3). Therefore, we did not consider these two minerals in our mantle melting calculations. We established two set of models based on the presence of garnet in the source, and ran 1000 Monte-Carlo simulations per model.

The first model assumes a garnet-free source, corresponding to the MSP with a lower *P-T* condition. Because only olivine and clinopyroxene are liquidus phase in this case, and at least ~20 wt.% of late-stage cumulate minerals (clinopyroxene and ilmenite) are required to effectively lower the melting temperature of the olivine-dominated source (Su et al., 2022; Tian et al., 2021), we limited the mineral mode of olivine in the mantle between 50 and 80 wt.% for this model, assuming

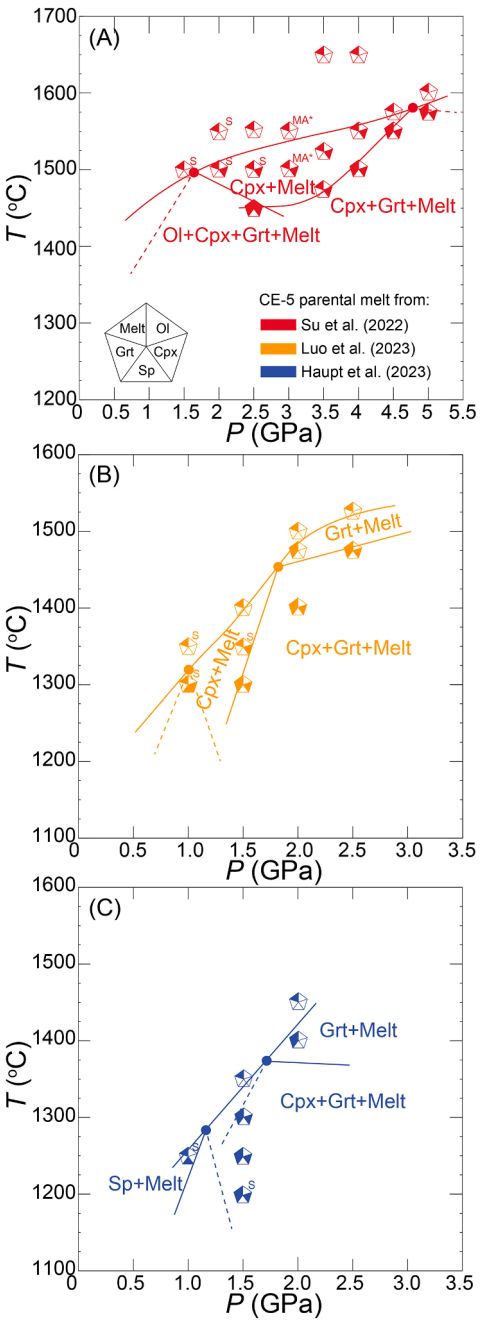

Fig. 3. High *P-T* experimental phase equilibria of three putative CE-5 parental melt compositions, showing the possible MSPs (solid circles) and phase boundaries (solid lines). Experiments with the letter "S" on the upper right are FeS-bearing experiments from Ji and Dasgupta (2025), with the "MA*" on the upper right, are experimental conditions conducted using both multi-anvil and piston cylinder device. A second MSP at a higher *P*-T is observed for all melt compositions in which garnet is a liquidus phase. Ol = olivine, Cpx = clinopyroxene, Grt = garnet, Sp = spinel, Melt=quenched silicate melt.

that the rest are clinopyroxene. The second model assumed a garnet-bearing source corresponding to the MSP at a higher *P-T* condition (Fig. 3), with clinopyroxene and garnet being the only two liquidus phases. Therefore, we limit the mode of garnet between 0 and 6 wt.%, and assume that the rest is clinopyroxene. Based on the PETROLOG modeling in Su et al. (2022), we assumed the crystallized mineral mode is 10% clinopyroxene with 90% of olivine. We plotted the composition of melts produced via 1–10% partial melting followed by 70% of fractional crystallization (methods described in Supplementary Materials), comparing the light REE $[(Ce/Sm)_{CI}]$ and heavy REE patterns $[(Dy/Yb)_{CI}]$ of modeled melts to CE-5 scooped soil, which was determined to contain very minor (<5%) exotic materials (Zong et al., 2022) and representative to the primitive CE-5 basalt (Wang et al., 2024a). The assumption of 70% fractional crystallization is arbitrary because the degree of fractional crystallization assumed here would minimally affect the REE pattern (Fig. S2). The results suggested that a olivine + clinopyroxene source without garnet generally fails to explain the heavy REE pattern of CE-5 scooped soil since the fractionation between Dy and Yb is too limited (cyan lines in Fig. 4A), while introducing a small amount of garnet (0 – 6 wt.%) in the clinopyroxene dominated source could efficiently fractionate heavy REEs and produce melts with compositional overlap with the average composition of CE-5 scooped soil (purple lines in Fig. 4A).

For all the garnet-bearing simulations plotted in Fig. 4A, we specifically recorded results parameters that yield $(Ce/Sm)_{CI}$ and $(Dy/Yb)_{CI}$ values of the melt that match those of CE-5 scooped soil within uncertainties (Fig. S3). In most successful simulations, the mineral fractions are ~95–98 wt.% clinopyroxene and ~2–5 wt.% garnet. In accordance with the above, we found that with 98 wt.% clinopyroxene and 2 wt.% garnet in the source, the REE pattern of CE-5 drilled soil, scooped soil, and basaltic clasts (Jiang et al., 2023; Wang et al., 2024c; Zong et al., 2022) can be well reproduced by 1–1.5% mantle melting followed by 67–80% of fractional crystallization (Fig. 4D).

Another possible petrogenesis of the CE-5 basalt is to generate the most primitive basalt by direct partial melting of the mantle source, followed by the fractional crystallization to reproduce more evolved basaltic fragments, in which case the mantle source consists mainly of clinopyroxene (Elardo et al., 2025; Haupt et al., 2023; Luo et al., 2023). Because this hypothesis lacks constraints on trace element abundances of the mantle source from previous studies, we constructed the mantle source based on clues provided by experiments and modeling regarding source mineral assemblages, assuming the minerals originally crystallized from the LMO. We followed the method described in Ji and Dygert (2023), assuming a LMO crystallized by the sequence reported in Charlier et al. (2018) with a Lunar Primitive Upper Mantle composition (LPUM; Longhi, 2006), in which model the olivine crystallized along with LMO solidified until 76 PCS, clinopyroxene joined the mineral assemblage after 82 PCS, and ilmenite crystallized only after 98 PCS, to calculate the trace element composition of each phase in the source. We assumed that, in each sequence, the mineral crystallized via Rayleigh fractionation, and that the initial bulk silicate Moon had a trace-element composition similar to 2.7 × CI chondrite (Fu and Jacobsen, 2024; Warren, 2005). We then performed Monte-Carlo simulations to explore the requirement for garnet in the source and constrained the olivine in the source to 0–30 wt.%, the ilmenite to 0–10 wt.%, and the remaining portion to clinopyroxene in the garnet-free source corresponding to the parental melt from Luo et al. (2023). Although we did not observe olivine as the crystallized mineral even at 1 GPa (B708; Table S2), we still assumed the potential presence of a certain amount of olivine in the mantle source to test the effect since the previous pMELTS simulations (Luo et al., 2023) suggested the MSP at lower *P-T* condition was primarily saturated with clinopyroxene with subordinate oxides and olivine. Similarly, for the parental melt composition from Haupt et al. (2023), we limited the ilmenite to 0–10 wt.%, and the rest were clinopyroxene in the garnet-free source, as neither in Haupt et al. (2023) nor the experimental results of this study observed olivine, orthopyroxene, or plagioclase as stable near-liquidus phases. In both scenarios of the garnet-bearing source modeling, we limited the garnet proportion to 0–6 wt.% with the remainder being clinopyroxene, to be consistent with previous assumptions. Wang et al. (2024c) suggested ~1–1.5 wt.% of KREEP component was required for the clinopyroxene-dominant mantle to reconcile the Sm-Nd isotopic characteristics of the CE-5 source. In all cases, we added the KREEP component from Warren (1989) after the construction of the source, limiting the proportion between 0 and 4 wt.% in the whole system. The trace element compositions of minerals in the

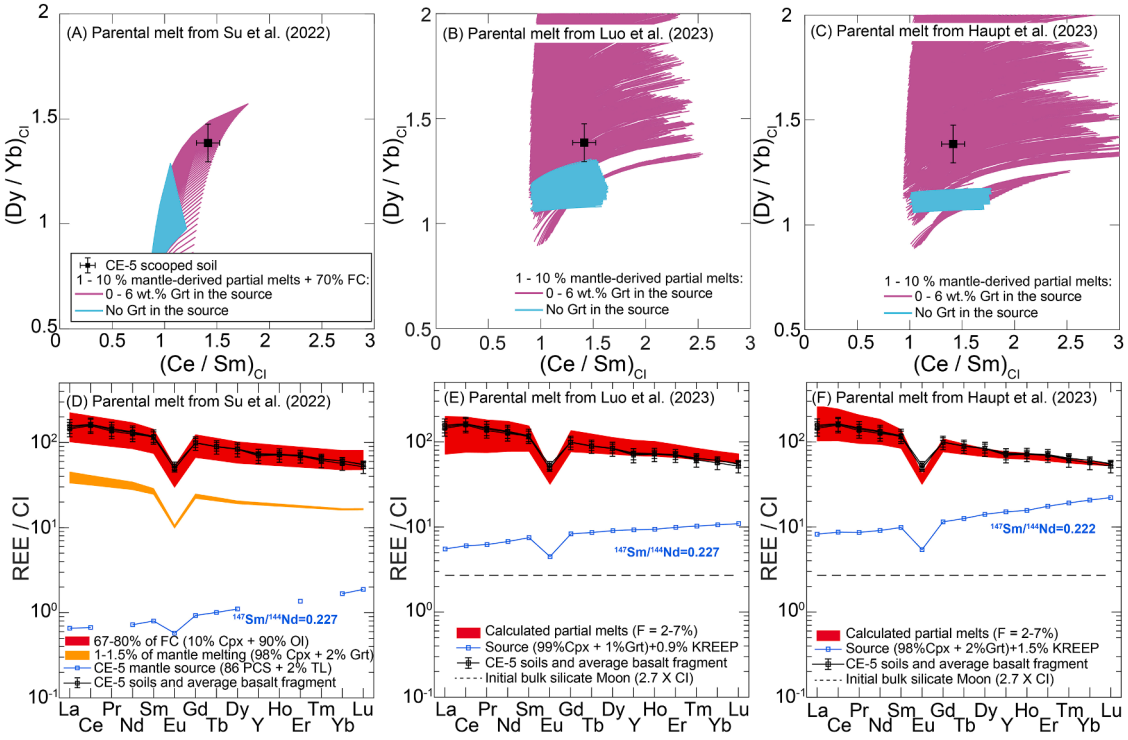

Fig. 4. Trace element modeling of three possible parental melt compositions regarding the petrogenesis of CE-5 mare basalts. The assumed trace element concentrations of the mantle source in panels A and D are from Tian et al. (2021), while the compositions of the mantle in panels B-C and E-F are calculated by Monte-Carlo simulation based on source mineral assemblages suggested by modeling (Luo et al., 2023) and experiments (this study; Haupt et al., 2023), as well as the isotopic constraint ($^{147}Sm/^{144}Nd$ = 0.222 – 0.227), assuming minerals are a direct crystallization product of a LMO with a 2.7 × CI chondrite trace element abundances (Fu and Jacobsen, 2024; Warren, 2005). In all scenarios, we can reproduce the REE pattern of the CE-5 drilled soil, scooped soil, and basaltic clasts with scenarios involving a clinopyroxene-dominant mantle source with small proportions of garnet, while the absence of garnet in the source fails to explain the REE pattern of the CE-5 sample (Fig. 4A-C). The compositions and 1σ errors of CE-5 drilled soil, scooped soil, and basaltic clasts are in the order from Wang et al. (2024c), Zong et al. (2022), and Jiang et al. (2023).

source were also determined by the Monte-Carlo method to originate from all possible PCS that are mainly composed of the target phases, i.e., the clinopyroxene in the source can crystallize from 82 to 98 PCS (high-Ca pyroxene-only cumulates after the plagioclase floatation), and olivine can be derived from 0 to 48 PCS (olivine-only cumulates; Charlier et al., 2018). The origin of garnet remains an open question. Garnet may be produced in situ, at shallower depths [e.g., during late-stage LMO cumulates sinking (Schmidt and Kraettli, 2022; Scholpp and Dygert, 2024)], or in the deeper mantle (Jing et al., 2022; Kraettli et al., 2022; Wood et al., 2024), and emplaced during LMO overturn. Therefore, we assumed that garnet could be in equilibrium with a stochastic LMO liquid, allowing us to set the absolute REE concentrations of garnet as a free parameter and attempt to constrain garnet's origin by documenting the sources of garnets in the successful simulations. Because we needed to construct the REE concentrations of the sources and filter out those that did not satisfy the Sm-Nd isotopic constraint ($^{147}Sm/^{144}Nd$ = 0.222 – 0.227; Tian et al., 2021), before further calculations, we performed further Monte-Carlo simulations (50,000) for garnet-free and garnet-bearing scenarios of both parental melt hypotheses. Subsequently, we calculated the compositions of the first 1–10% modal batch melts for all qualified source compositions. For both parental melt hypotheses, the melts from garnet-free sources fail to reproduce the $(Dy/Yb)_{CI}$ of the CE-5 scooped soil, even considering the addition of KREEP component (cyan lines in Fig. 4B-C), while the addition of garnet in the clinopyroxene dominant source could efficiently fractionate the heavy REE in the melts and produce the REE pattern of CE-5 sample within the uncertainties (purple lines in Fig. 4B-C). The recorded successful simulations (Figs. S4-S5) suggested that garnet-bearing pyroxenitic sources with ~1–3 wt.% of KREEP component were able to reproduce the REE pattern of CE-5 soils, and basaltic clasts after 2–7% of melting (Fig. 4E-F). We note that our Monte-Carlo simulations do indicate multiple possibilities for the LMO cumulate source of garnet (82 – 99 PCS), as well as its percentage within the source (~0.5 – 4 wt.%; Figs. S4-S5). In other words, while our trace element modeling does demonstrate that garnet's presence in the mantle source is essential, it fails to effectively constrain the origin of garnet in the young lunar mantle. The origin of garnet in the CE-5 mantle source will be discussed in a later section.

Elardo et al. (2025) proposed that the source of CE-5 mare basalt should be a shallow (75 – 130 km) plagioclase-bearing mantle. However, even their own trace-element model shows unsatisfactory fit to the REE pattern of the CE-5 basalt for both light and heavy REEs. Here, we applied the trace-element modeling methods described above to test whether partial melting of a plagioclase-bearing mantle can reproduce the CE-5 basalts. Since our experiment did not cover pressures below 1 GPa, we directly used the MSP (~0.5 GPa, 1200 °C) and mineral assemblage (10% ilmenite, 5% olivine, 5% plagioclase, and 80% clinopyroxene) suggested by Elardo et al. (2025). Even though we assumed that the mineral assemblage may originate from all possible PCS of LMO cumulates and allow the addition of KREEP component, that the heavy REE pattern of modeled melts $[(Dy/Yb)_{CI}]$ still fail to match that of the CE-5 basalt (Fig. 5). The above calculations further support, from the perspective of trace elements, that garnet must exist in the source region of CE-5 basalt.

4.3. *The garnet-free mantle source of Apollo 12002 basalt*

Investigating whether garnet was also present in the sources of older Apollo basalts to reconcile their trace-element signatures could help us track the geodynamic evolution of the lunar mantle. We chose Apollo

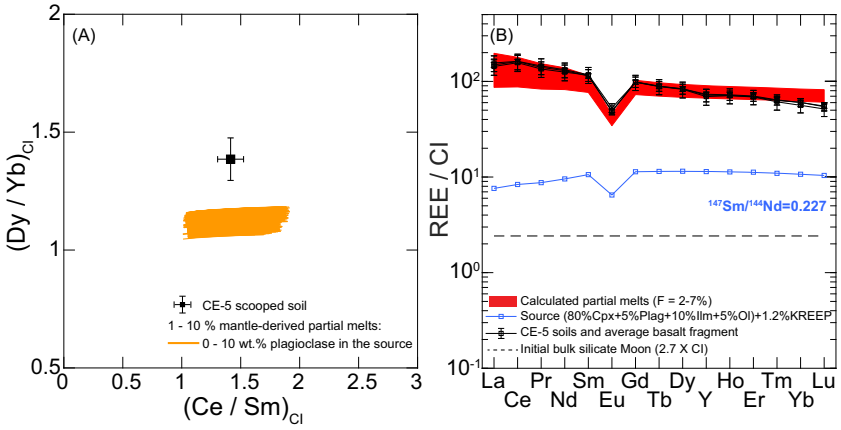

Fig. 5. Trace element modeling of mantle melting of a garnet-free, plagioclase-bearing mantle source. (A) The modeling of the mantle-derived partial melts compositions by Monte-Carlo simulations. The methods are the same as those applied in Fig. 4. (B) The whole REE pattern of the mantle-derived partial melts by applying the source mineral assemblage and melting degree suggested by Elardo et al. (2025). None of the scenarios reproduce the heavy REE pattern $[(Dy/Yb)_{CI}]$ of the CE-5 drilled soil, scooped soil, and basaltic clasts with scenarios involving the clinopyroxene-dominant mantle source containing small proportions of plagioclase.

12002 low-Ti basalt because previous studies have proposed that they may originate from a similar source region as CE-5 basalt due to the similarities in major elements (Luo et al., 2023) and isotopic characteristics (Tian et al., 2021). In addition, Apollo 12002 was considered a good representative of primitive mantle-derived products (Grove et al., 1973; Walker et al., 1976). We applied the same trace-element modeling method and constructed their sources based on the phase diagram in Grove et al. (1973), which suggested that the experimental MSP of 12002 basalts was ~1.3 GPa and 1380 °C, and that olivine, clinopyroxene, and spinel were liquidus phases. We applied the modeling method described above, which assumed the source minerals originally crystallized from the LMO and filtered out sources that did not meet the isotopic criteria. Then we simulated the mantle melting process. The results indicated that garnet is not a required phase in the mantle source of the Apollo 12002 low-Ti basalt and that its REE pattern can be reproduced by a higher degree of melting (10–30%) of a mantle source with 65 wt.% olivine + 35 wt.% clinopyroxene and the addition of a 0.9 wt.% KREEP component (Figs. S6).

5. The evaluation of three putative parental melt compositions and the corresponding petrogenesis of the CE-5 basalt

Garnet is required in the CE-5 mantle source by our trace element modeling and also shown to be a possible liquidus phase for partial melts parental to CE-5 basalts. We subsequently evaluate the three applied parental melt compositions to constrain the source lithology. If none of the primitive CE-5 clasts can represent the mantle-derived parental melt composition and CE-5 parental melt experienced extensive fractional crystallization of olivine and/or orthopyroxene after mantle melting, as proposed by Su et al. (2022), the MSP with the garnet at the liquidus is very deep (~4.75 GPa; Fig. 3A) for this primitive melt. Such a high pressure corresponds to ~1300 km depth in the lunar mantle, placing the condition within a partially melted low-velocity zone (LVZ) at the core-mantle boundary (e.g., Khan et al., 2014; Weber et al., 2011). However, only the Ti-enriched melt (e.g., ~16 wt.% of TiO_2; van Kan Parker et al., 2012) can remain neutrally buoyant at such depth, and 3 – 16 vol.% of Fe-Ti oxides are required in the residue (Pommier et al., 2024), probably as a consequence of the sinking of the ilmenite-bearing cumulates during lunar mantle overturn. Based on the possible garnet-bearing mantle lithology (Fig. 3), the source of the CE-5 mare basalt can neither be in equilibrium with ilmenite nor coexist with such a high-Ti melt. Furthermore, according to PETROLOG simulations in Su et al. (2022), the fractional crystallization products of this primitive parental melt composition under low pressure are olivine and orthopyroxene. Nevertheless, the lack of olivine or orthopyroxene phenocrysts that could be in equilibrium with the melt of relatively high Mg# (>32; Elardo et al., 2025) may also suggest the limited olivine ± orthopyroxene crystallization after mantle melting. The low-temperature experiments by Elardo et al. (2025) also suggested that neither olivine nor orthopyroxene is the liquidus phase at the potential magma-chamber pressure range (e.g., ~0.2–0.5 GPa; Luo et al., 2023). Therefore, we do not further consider the scenario that the CE-5 mantle source is located at the lunar core-mantle boundary.

The parental melt composition selected by Luo et al. (2023) is the basaltic clast with the highest Mg# (~47) and the lowest TiO_2 concentration, which is likely the most primitive melt prior to subsequent fractional crystallization and is more representative of the mantle-derived parental melt. Elardo et al. (2025) evaluated a range of CE-5 basaltic clasts by the olivine-melt Fe-Mg exchange coefficients and chose a clast that shows great similarities with the parental melt recommended by Haupt et al. (2023) regarding the major element compositions (Fig. 1). The MSPs involving garnet for initial compositions from both Luo et al. (2023) and Haupt et al. (2023) show a consistent pressure (~1.75 GPa) and a narrow temperature range, from 1375 to 1450 °C. If the primitive CE-5 basalts were generated by direct mantle melting, then the mantle source should be garnet-bearing clinopyroxenite at a depth of ~350 km. This scenario is most consistent with all geochemical and experimental constraints.

6. The origin of the garnet in the mantle source

The speculations about the presence of garnets in the lunar interior are decades old and several previous studies proposed that the garnet-bearing lunar mantle can help explain some lunar interior geophysical observations (Kuskov and Kronrod, 1998; Wood et al., 2024), as well as elemental fractionation, such as Lu/Hf and Sm/Yb, in the Apollo mare basalts and volcanic glasses (Barr and Grove, 2013; Beard et al., 1998; Neal, 2001; Scholpp and Dygert, 2026). Recent modeling and experiments investigating the LMO solidification process suggested that garnet can only crystallize from LMO at pressure > 3.5 GPa (Jing et al., 2022; Kraettli et al., 2022). This pressure is deeper than the MSPs for the CE-5 parental melt suggested by Luo et al. (2023) and Haupt et al. (2023), but is consistent with the deep origin suggested by the MSP of parental melt from Su et al. (2022). However, the hypothesis of garnet directly crystallized from LMO is based on the premise that the bulk silicate Moon is relatively Al-enriched (i.e., the Taylor Whole Moon; Taylor, 1982), an assumption that makes it difficult to reconcile the thickness of the lunar crust (e.g., Elardo et al., 2011; Taylor and Wieczorek, 2014). In addition,

if garnet is the product of direct LMO crystallization, all subsequent cumulates crystallized from the remaining liquid and their melting products would exhibit relative depletion of heavy REE. However, such an REE pattern is not widely observed in lunar samples (Li et al., 2025). Rationalizing this difference requires a scenario, such as a basal LMO to isolate the garnet from relatively shallower LMO cumulates (e.g., Kraettli et al., 2022), which makes the origin of garnet overly dependent on a specific LMO evolution model and bulk silicate Moon initial compositions.

Observations from some studies can also be interpreted to argue that under high-pressure conditions, the lunar hybridized mantle can stabilize garnet (e.g., Mallik et al., 2019; Scholpp and Dygert, 2024). Johnson et al. (2021) also suggested that lunar primitive mantle melting could occur in the garnet stability field at pressures >~2 GPa and temperatures >~1400 °C. Therefore, if the CE-5 parental melt was indeed in equilibrium with garnet, then introducing relatively fertile shallow components into the deep mantle to stabilize garnet seems to be a more feasible solution.

The Rb and Sr isotopic data of CE-5 plagioclase indicated that the source region of the CE-5 basalt should show $^{87}Rb/^{86}Sr$ ratios around 0.009 to 0.022 (Tian et al., 2021). Similar $^{87}Rb/^{86}Sr$ ratios in the lunar mantle have previously been explained by ~2% of plagioclase trapped in the relatively late-stage cumulate (78 – 95 PCS; Borg et al., 2009). Elardo et al. (2025) therefore pointed out that the Rb-Sr isotopic characteristics of CE-5 basalts provide important evidence supporting the presence of plagioclase, rather than garnet, in the mantle source. On the contrary, the trace element modeling by Zong et al. (2022) suggested that the clinopyroxene-dominant cumulate with a small amount of KREEP can also satisfy the Rb-Sr and Sm-Nd isotopic signatures of the CE-5 mantle source. Compared to the REEs, the predictive uncertainties associated with Rb and Sr partitioning are substantially larger, owing to the lack of predictive modeling of Rb partitioning for almost all LMO crystallization minerals except plagioclase (Sun et al., 2017), and the absence of Sr partitioning model of garnet, ilmenite, and olivine. Likewise, the recently reported $^{176}Lu/^{177}Hf$ isotopic ratios for the CE-5 source can further constrain the mantle lithology in our trace-element modeling. However, there is currently no reliable predictive partitioning model of Hf for olivine, plagioclase, or garnet. As a first-order estimate, we calculated the concentrations of Hf, Rb, and Sr in the garnet-bearing source region and primary mantle melts applying the same method as for REEs, with partition coefficients of Hf, Rb and Sr calculated by predictive models and selected from lunar-relevant studies (Table S3), assuming the CE-5 parental melt has the composition recommended by Luo et al. (2023) (same as modeling in Fig. 4E; more details are provided in the Supplementary Materials). The results indicate the Lu-Hf, Rb-Sr, and Sm-Nd isotopic ratios of the garnet-bearing source all fall within the required range reported by Tian et al. (2021), and match the values measured for CE-5 basalt clast (Shen et al., 2025; Fig. S7). Furthermore, the resulting primitive mantle melt can reproduce the REE, Hf, Rb, and Sr concentrations of the CE-5 samples (Fig. S7). Our modeling also demonstrates that the Rb–Sr isotopic characteristics of CE-5 basalts cannot be used to rule out garnet in the source. However, due to the lack of *P*-, *T*-, and composition-dependent partitioning models of Hf, Rb, and Sr, we do not present the evolution of these elements in trace element modeling in the main text, in order to avoid propagating unevaluated uncertainties.

Although our modeling indicates a garnet-bearing source is feasible, the presence of plagioclase in the mantle can also result in a lower $^{87}Rb/^{86}Sr$ source, as the Sr strongly prefers to partition into plagioclase rather than other LMO crystallization phases. The ~2% plagioclase in the source suggested by Borg et al. (2009) coincides with the proportion of garnet in the source according to our modeling (Figs. S3-S5), suggesting that garnet may have formed through the metamorphism of plagioclase-bearing clinopyroxenitic cumulate upon sinking to deeper depths such as following reaction:

plagioclase + clinopyroxene 1 ± ilmenite = garnet + clinopyroxene 2 ± melt (1)

Reactions that are similar with Eq. (1) has been widely applied to describe the garnet stabilizing process in both terrestrial and lunar environment at super- (e.g., Springer and Seck, 1997; Schmidt and Kraettli, 2022) or sub-solidus conditions (e.g., Roy Choudhury et al., 2023; Chatterjee et al., 2023; Scholpp and Dygert, 2024), which could exhaust all the plagioclase and potential oxides (e.g., ilmenite) from the source, ultimately leaving only clinopyroxene and garnet as the residual minerals in the mantle. If the garnet-bearing CE-5 mantle source formed by metamorphism of plagioclase-bearing pyroxenite, then the mantle could preserve the Sr-isotopic signature of the protolith and therefore exhibit a relatively low $^{87}Rb/^{86}Sr$ ratio. In addition to the mechanism above (Eq. (1)), ilmenite and plagioclase can also be removed by partial melting of the mantle source before the generation of CE-5 parental melt. Therefore, only garnet and clinopyroxene were present in the mantle residue, as demonstrated by our experimental phase equilibria (Fig. 3). Consequently, it is reasonable to exclude plagioclase and ilmenite in our trace element modeling.

The garnet formation process described by Eq. (1) is also able to explain the Ti-enriched signature of parental melt proposed by Haupt et al. (2023) (~2.5 wt.% higher TiO_2 than the other two putative parental melts applied; Fig. 1D). Our experiments suggested the minerals that are in equilibrium with this relative Ti-enriched melt also show higher TiO_2 concentrations (~1.82–2.05 wt.% in clinopyroxene and 1.41–1.70 wt.% in garnet). This observation is consistent with the experiments constraining the metamorphic phase relationship of ilmenite-bearing cumulates (15% ilmenite + 85% of clinopyroxene) during lunar mantle overturn (Scholpp and Dygert, 2024). According to Scholpp and Dygert (2024), garnet and clinopyroxene that result from high pressure transformation of ilmenite-bearing cumulates have TiO_2 concentration of 2.38 – 3.45 wt.% and 1.66 – 2.32 wt.%, respectively. Hoyos and Grove (2023) suggested the high-Ti primitive melt (e.g., Elardo et al., 2025; Haupt et al., 2023; Fig. 1D) is the parental melt of a small number of high-Ti CE-5 basaltic clasts (n = 6) before undergoing fractional crystallization of olivine and plagioclase. If that is the case, the formation of such mantle source will require a lesser removal of Ti-enriched phase during overturn or relative higher proportion of ilmenite in the pre-overturn lunar mantle compared to the parental melt proposed by Luo et al. (2023). We also note that the scenario in which the Ti-enriched parental melts suggested by Haupt et al. (2023) and Elardo et al. (2025) (TiO_2 = 5.7 – 7.0 wt.%) are not derived from the primitive mantle cannot be ruled out, because a more compelling explanation for the generation of this relatively high-Ti magma involves processes occurring after mantle melting, such as fractional crystallization (e.g., Hoyos and Grove, 2023), magma mixing, assimilation of ilmenite-bearing cumulate (e.g., Shearer and Papike, 1999; Wagner and Grove, 1997), or magmatic recharge (e.g., Ji et al., 2026). Evaluating the magmatic differentiation processes that CE-5 parental melt may have experienced is beyond the scope of this study, and we, therefore, do not extend this discussion further. Interestingly, our experiments using the parental melt suggested by Haupt et al. (2023) indicate that a garnet-bearing mantle generated by metamorphism of late-stage plagioclase and ilmenite-bearing cumulates, can generate moderate-high TiO_2 signature in primitive melt (G866, G872, and B669; Table S2), and the primitive melt could exhibit even higher TiO_2 concentration before ilmenite was completely consumed (e.g., Scholpp and Dygert, 2024).

7. Geodynamic implications

Based on both laboratory-based phase equilibria experiments and accompanying trace element modeling, we suggest that the source of young CE-5 magma contains garnet. Furthermore, among all the possible scenarios of garnet in the source, a garnet-clinopyroxenite

source at the mid-mantle depth satisfies most constraints. However, our modeling suggested that a garnet-bearing source region of Apollo 12002 (~260 km; Fig. 6A) is not required, an intriguing difference from the younger CE-5 mantle. If this difference represents mantle heterogeneity, then garnet in the CE-5 source region might be the result of LMO cumulate overturn, since the clinopyroxene-rich mineralogic assemblage with aluminous component could only represent the late-stage LMO solidification products [e.g., ~100 km (Charlier et al., 2018; Lin et al., 2017; Snyder et al., 1992)], which is inconsistent with the pressures of garnet-present MSP (~350 km; Fig. 3) and, therefore, requires a process, to introduce the late-stage LMO products (clinopyroxenite, ilmenite, and minor KREEP component) into the deep mantle. The presence of garnet in the source once again suggests the crucial role of overturn. The cumulate mantle overturn was triggered by density instability (Elkins-Tanton et al., 2011; Hess and Parmentier, 1995), and the downwelling of the late-stage LMO cumulates was able to stabilize garnets during the process (Schmidt and Kraettli, 2022; Scholpp and Dygert, 2024). The garnet-clinopyroxenite source of CE-5 can be generated via sinking of the dense ilmenite-bearing cumulate layer, while the Ti-rich phase in the mantle could be stripped off gradually either via early-stage partial fusion of the mantle source, grain-scale density stripping, or be exhausted with plagioclase in the metamorphic reaction during sinking (Eq. 1; Fig. 6B) so as to generate the more Ti-enriched parental melt. Furthermore, even if the primitive source is a clinopyroxene-plagioclase-bearing cumulate, regardless of whether the ilmenite in it is present or completely exhausted, its density will still be higher than underlying early-stage olivine-dominant cumulates (Elkins-Tanton et al., 2011). Therefore, in the case of overturn caused by density instability, even without the direct involvement of ilmenite, the clinopyroxenite source would still sink to the deep mantle together with ilmenite-bearing cumulate due to the density difference. Our Monte Carlo simulation supported this theory, as garnet in the CE-5 source was more likely to have originated from late-stage LMO cumulates (Figs. S4D and S5D).

Interestingly, the Apollo 12002 low-Ti basalt does not show evidence of garnet in its source. If Apollo 12002 low-Ti basalt and CE-5 basalt originated from a similar mantle, the difference in their source mineral assemblages could also be indicative of a late-stage process to implant significant fertile components into the deeper lunar mantle after ~3.2 Ga (age of Apollo 12002 basalts; Turner, 1971), which would generate the second-stage garnet-bearing, pyroxenitic mantle, as documented in the Earth's mantle (Kelemen et al., 1998). Alternatively, if the source region of CE-5 basalts formed during the LMO overturn, it suggests that the extent of LMO overturn was not similar across the whole Moon. Apollo samples, especially for high-Ti basalts, show evidence of containing an ilmenite-bearing cumulate layer and KREEP (Brown and Grove, 2015; Kommescher et al., 2020), whereas CE-5 samples show a greater requirement for the introduction of a plagioclase-bearing clinopyroxenitic cumulate, while the other fertile components (i.e., ilmenite) could be consumed during the lunar mantle overturn (e.g., Eq. (1)) or during the early-stage of mantle melting (Fig. 6B).

CRediT authorship contribution statement

Dian Ji: Writing – review & editing, Writing – original draft, Methodology, Investigation, Formal analysis, Data curation. **Rajdeep Dasgupta:** Writing – review & editing, Validation, Supervision, Methodology, Funding acquisition, Conceptualization.

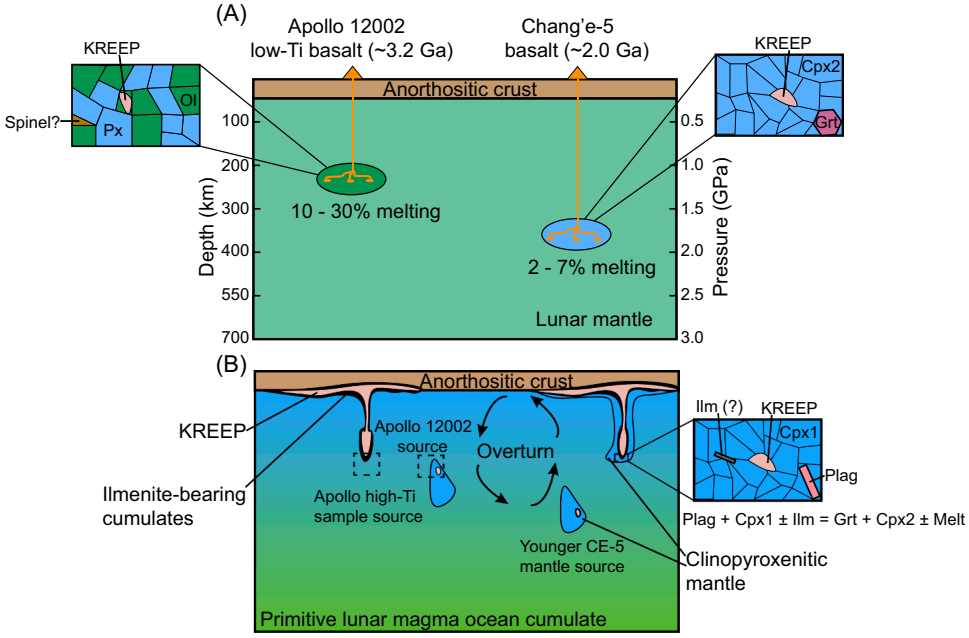

Fig. 6. (A) A schematic illustrating the possible location and mineral assemblage in the mantle source of CE-5 and Apollo 12002 mare basalts. The CE-5 mare basalts are generated by 2 – 7 wt.% partial melting of a mantle source (~350 km), and the source must contain garnet and ~1 – 3 wt.% KREEP component to reconcile the REE pattern of primitive CE-5 basalt and the Sm-Nd isotopic character of the mantle. In contrast, the mantle of Apollo 12002 low-Ti basalt (~260 km), which is suspected to originate from the same source region as CE-5 according to previous studies (Luo et al., 2023), did not require the presence of garnet, which may suggest either that the two came from different source regions, or at least the mineralogic characteristics of the two are different, with the CE-5 source having a greater, fusible component. (B) A possible scenario of lunar cumulate overturns, which may have shaped the source of Apollo and CE-5 mare basalts. For Apollo high-Ti basalt and glass, experimental (Brown and Grove, 2015) and isotopic (Kommescher et al., 2020) studies suggest an origin from a hybridized source contaminated by the KREEP component and ilmenite, which could have formed through the downwelling of ilmenite-bearing cumulates during lunar mantle cumulate overturn. However, this overturn could also serve as a mechanism for garnet formation in the source of CE-5 basalts. The denser clinopyroxene-dominant cumulates + plagioclase ± ilmenite (compared to the early crystallized olivine-dominant cumulates; Elkins-Tanton et al., 2011) would also descend during the overturn. Additionally, small amounts of plagioclase (~1 – 2 wt.%) and any potential oxides trapped in the cumulates would react with clinopyroxene (>1 GPa; Schmidt and Kraettli, 2022) to stabilize garnet. The formation of the hybridized source of Apollo 12002 low-Ti basalt also requires overturn, in which the downwelling KREEP-bearing clinopyroxenite is mixed with the upwelling or local olivine-dominant cumulate and stays at the relatively shallow depths (~260 km).

Declaration of competing interest

The authors declare that they have no known competing financial interests or personal relationships that could have appeared to influence the work reported in this paper.

Acknowledgments

We thank Gelu Costin and Kenneth Befus for their help with electron microprobe analysis. We thank Denim-Leenox Sasser for the assistance during the experiments, as well as Proteek Chowdhury and Bidong Zhang for the helpful discussions. The effective editorial handling by Fang-Zhen Teng, as well as the constructive comments from two anonymous reviewers, are greatly appreciated. This work was supported by NASA grant 80NSSC18K0828 to RD. DJ acknowledges a graduate fellowship from the Rice Space Institute Center for Planetary Origins to Habitability (CPO2H).

Supplementary materials

Supplementary material associated with this article can be found, in the online version, at doi:10.1016/j.epsl.2026.120133.

Data availability

All data are reported in the paper and provided in the supplementary materials.

References

Astudillo Manosalva, D.F., Elardo, S.M., 2024. Assessing the accuracy of phase equilibrium software in reproducing the liquidus multiple saturation conditions of lunar and martian basalt compositions. Meteorit. Planet. Sci. 59, 260–285.
Barr, J.A., Grove, T.L., 2013. Experimental petrology of the Apollo 15 group A green glasses: melting primordial lunar mantle and magma ocean cumulate assimilation. Geochim. Cosmochim. Acta 106, 216–230.
Beard, B.L., Taylor, L.A., Scherer, E.E., Johnson, C.M., Snyder, G.A., 1998. The source region and melting mineralogy of high-titanium and low-titanium lunar basalts deduced from Lu-Hf isotope data. Geochim. Cosmochim. Acta 62, 525–544.
Borg, L.E., Gaffney, A.M., Shearer, C.K., DePaolo, D.J., Hutcheon, I.D., Owens, T.L., Ramon, E., Brennecka, G., 2009. Mechanisms for incompatible-element enrichment on the Moon deduced from the lunar basaltic meteorite Northwest Africa 032. Geochim. Cosmochim. Acta 73, 3963–3980.
Brown, S., Grove, T., 2015. Origin of the Apollo 14, 15, and 17 yellow ultramafic glasses by mixing of deep cumulate remelts. Geochim. Cosmochim. Acta 171, 201–215.
Carter, L.B., Dasgupta, R., 2015. Hydrous basalt–limestone interaction at crustal conditions: implications for generation of ultracalcic melts and outflux of CO2 at volcanic arcs. Earth Planet. Sci. Lett. 427, 202–214.
Castillo, P.R., 2012. Adakite petrogenesis. Lithos 134-135, 304–316.
Charlier, B., Grove, T.L., Namur, O., Holtz, F., 2018. Crystallization of the lunar magma ocean and the primordial mantle-crust differentiation of the Moon. Geochim. Cosmochim. Acta 234, 50–69.
Chatterjee, S., Karmakar, S., Mukherjee, S., Sanyal, S., Sengupta, P., 2023. Origin of clinopyroxene-ilmenite symplectites in mafic granulites from eastern parts of the Chotanagpur granite gneissic complex, East Indian shield. Am. Mineral. 108, 2308–2322.
Che, X., Nemchin, A., Liu, D., Long, T., Wang, C., Norman, M.D., Joy, K.H., Tartese, R., Head, J., Jolliff, B., 2021. Age and composition of young basalts on the Moon, measured from samples returned by Chang'e-5. Science 374, 887–890.
Chen, Y., Hu, S., Li, J.-H., Li, Q.-L., Li, X., Li, Y., Liu, Y., Qian, Y., Yang, W., Zhou, Q., 2023. Chang'e-5 lunar samples shed new light on the Moon. Innov. Geosci. 1, 100014, 100014-100011-100014-100015.
Ding, S., Dasgupta, R., Tsuno, K., 2014. Sulfur concentration of martian basalts at sulfide saturation at high pressures and temperatures – Implications for deep sulfur cycle on Mars. Geochim. Cosmochim. Acta 131, 227–246.
Ding, S., Hough, T., Dasgupta, R., 2018. New high pressure experiments on sulfide saturation of high-FeO* basalts with variable TiO2 contents–Implications for the sulfur inventory of the lunar interior. Geochim. Cosmochim. Acta 222, 319–339.
Dygert, N., Ji, D., Etheridge, E.N., 2025. A predictive model for divalent element partitioning between clinopyroxene and basaltic melt and an europium-in-plagioclase-clinopyroxene oxybarometer for cumulate rocks. Geochim. Cosmochim. Acta. 394, 148–163.
Elardo, S.M., Cone, K.A., Siegler, M.A., Williams, S.J., Palin, R.M., 2025. A shallow mantle source for the Chang'e 5 lavas reveals how top-down heating prolonged lunar magmatism. Sci. Adv. 11, eadr1486.
Elardo, S.M., Draper, D.S., Shearer Jr, C.K., 2011. Lunar Magma Ocean crystallization revisited: bulk composition, early cumulate mineralogy, and the source regions of the highlands Mg-suite. Geochim. Cosmochim. Acta 75, 3024–3045.
Elkins-Tanton, L.T., Burgess, S., Yin, Q.Z., 2011. The lunar magma ocean: reconciling the solidification process with lunar petrology and geochronology. Earth Planet. Sci. Lett. 304, 326–336.
Filiberto, J., Dasgupta, R., 2011. Fe2+–Mg partitioning between olivine and basaltic melts: applications to genesis of olivine-phyric shergottites and conditions of melting in the Martian interior. Earth Planet. Sci. Lett. 304, 527–537.
Filiberto, J., Dasgupta, R., 2015. Constraints on the depth and thermal vigor of melting in the Martian mantle. J. Geophys. Res.: Planets 120, 109–122.
Fu, H., Jacobsen, S.B., 2024. Earth-moon refractory element similarity constrains a thoroughly-mixed Moon-forming disk. Earth Planet. Sci. Lett. 646, 119008.
Green, D., Ringwood, A., Hibberson, W., Ware, N., 1975. Experimental petrology of Apollo 17 mare basalts. In: Lunar Science Conference, 6th, Houston, Tex., March 17-21, 1975, Proceedings, 1. Research supported by the California Institute of Technology, pp. 871–893 (A78-46603 21-91) New York, Pergamon Press, Inc., 1975, p. 871-893.
Grove, T., Walker, D., Longhi, J., Stolper, E., Hays, J., 1973. Petrology of 12002 and the origin of picritic basalts. In: Proc. 4. Lunar Sci. Conf, pp. 995–1011.
Haupt, C., Renggli, C., Klaver, M., Steenstra, E., Berndt, J., Rohrbach, A., Klemme, S., 2023. Experimental and petrological investigations into the origin of the lunar Chang'e 5 basalts. Icarus 402, 115625.
He, Q., Li, Y., Baziotis, I., Qian, Y., Xiao, L., Wang, Z., Zhang, W., Luo, B., Neal, C.R., Day, J.M., 2022. Detailed petrogenesis of the unsampled Oceanus Procellarum: the case of the Chang'e-5 mare basalts. Icarus 383, 115082.
Herzberg, C., Condie, K., Korenaga, J., 2010. Thermal history of the Earth and its petrological expression. Earth Planet. Sci. Lett. 292, 79–88.
Hess, P.C., Parmentier, E., 1995. A model for the thermal and chemical evolution of the Moon's interior: implications for the onset of mare volcanism. Earth Planet. Sci. Lett. 134, 501–514.
Hoyos, S., Grove, T., 2023. Petrogenesis of the Chang'E-5 mare basalts: implications for the origin of the youngest sampled lunar magmas. LPI Contributions 2806, 1858.
Ji, D., Dasgupta, R., 2025. Sulfur inventory of the young lunar mantle constrained by experimental sulfide saturation of Chang'e-5 mare basalts and a new sulfur solubility model for silicate melts in equilibrium with sulfides of variable metal–sulfur ratio. Geochim. Cosmochim. Acta. 394, 284–297.
Ji, D., Dasgupta, R., Lee, C.-T., 2026. The effects of magmatic recharge on primary lunar melt compositions: implications for the water and other volatile budget of the Moon. Geochim. Cosmochim. Acta 420, 131–147.
Ji, D., Dygert, N., 2023. Trace element evidence for serial processing of the lunar flotation crust and a depleted bulk Moon. Earth Planet. Sci. Lett. 602, 117958.
Ji, D., Dygert, N., 2024. Trace element partitioning between apatite and silicate melts: effects of major element composition, temperature, and oxygen fugacity, and implications for the volatile element budget of the lunar magma ocean. Geochim. Cosmochim. Acta 369, 141–159.
Jiang, Y., Kang, J., Liao, S., Elardo, S.M., Zong, K., Wang, S., Nie, C., Li, P., Yin, Z., Huang, F., 2023. Fe and Mg isotope compositions indicate a hybrid mantle source for young Chang'E 5 mare basalts. Astrophys. J. Lett. 945, L26.
Jing, J.-J., Lin, Y., Knibbe, J.S., van Westrenen, W., 2022. Garnet stability in the deep lunar mantle: constraints on the physics and chemistry of the interior of the Moon. Earth Planet. Sci. Lett. 584, 117491.
Johnson, T., Morrissey, L., Nemchin, A., Gardiner, N., Snape, J., 2021. The phases of the Moon: modelling crystallisation of the lunar magma ocean through equilibrium thermodynamics. Earth Planet. Sci. Lett. 556, 116721.
Kelemen, P.B., Hart, S.R., Bernstein, S., 1998. Silica enrichment in the continental upper mantle via melt/rock reaction. Earth Planet. Sci. Lett. 164, 387–406.
Khan, A., Connolly, J.A., Pommier, A., Noir, J., 2014. Geophysical evidence for melt in the deep lunar interior and implications for lunar evolution. J. Geophys. Res: Planets 119, 2197–2221.
Kommescher, S., Fonseca, R.O., Kurzweil, F., Thiemens, M., Münker, C., Sprung, P., 2020. Unravelling lunar mantle source processes via the Ti isotope composition of lunar basalts. Geochem. Perspect. Lett. 13, 13–18.
Kraettli, G., Schmidt, M.W., Liebske, C., 2022. Fractional crystallization of a basal lunar magma ocean: a dense melt-bearing garnetite layer above the core? Icarus 371, 114699.
Krawczynski, M.J., Grove, T.L., 2012. Experimental investigation of the influence of oxygen fugacity on the source depths for high titanium lunar ultramafic magmas. Geochim. Cosmochim. Acta 79, 1–19.
Kuskov, O., Kronrod, V., 1998. Constitution of the moon: 5. Constraints on composition, density, temperature, and radius of a core. Phys. Earth Planet. Inter. 107, 285–306.
Li, Q.-L., Zhou, Q., Liu, Y., Xiao, Z., Lin, Y., Li, J.-H., Ma, H.-X., Tang, G.-Q., Guo, S., Tang, X., 2021. Two-billion-year-old volcanism on the Moon from Chang'e-5 basalts. Nature 600, 54–58.
Li, R., Tang, M., Wang, J., 2025. A lower mantle origin for the young mare basalts returned by Chang'e-5? Earth Planet. Sci. Lett. 671, 119650.
Lin, Y., Tronche, E.J., Steenstra, E.S., Van Westrenen, W., 2017. Experimental constraints on the solidification of a nominally dry lunar magma ocean. Earth Planet. Sci. Lett. 471, 104–116.
Longhi, J., 2006. Petrogenesis of picritic mare magmas: constraints on the extent of early lunar differentiation. Geochim. Cosmochim. Acta 70, 5919–5934.
Luo, B., Wang, Z., Song, J., Qian, Y., He, Q., Li, Y., Head, J.W., Moynier, F., Xiao, L., Becker, H., 2023. The magmatic architecture and evolution of the Chang'e-5 lunar basalts. Nat. Geosci. 16, 301–308.

Mallik, A., Ejaz, T., Shcheka, S., Garapic, G., 2019. A petrologic study on the effect of mantle overturn: implications for evolution of the lunar interior. Geochim. Cosmochim. Acta 250, 238–250.
McCubbin, F.M., Vander Kaaden, K.E., Tartèse, R., Boyce, J.W., Mikhail, S., Whitson, E. S., Bell, A.S., Anand, M., Franchi, I.A., Wang, J., 2015. Experimental investigation of F, Cl, and OH partitioning between apatite and Fe-rich basaltic melt at 1.0–1.2 GPa and 950–1000 C. Am. Mineral. 100, 1790–1802.
Moitra, H., Ghosh, S., Mukherjee, T., Gupta, S., Marhas, K.K., 2026. Interaction between ilmenite-bearing cumulates and lunar mantle: implications for the origin of intermediate and high-titanium lunar basalts. Geochim. Cosmochim. Acta 421, 196–213.
Neal, C.R., 2001. Interior of the Moon: the presence of garnet in the primitive deep lunar mantle. J. Geophys. Res.: Planets 106, 27865–27885.
Pal, A., Dasgupta, R., 2024. The fate of nitrogen during early silicate differentiation of rocky bodies constrained by experimental mineral-melt partitioning. Geochim. Cosmochim. Acta 385, 45–60.
Pommier, A., Walter, M.J., Hao, M., Yang, J., Hrubiak, R., 2024. Acoustic and electrical properties of Fe-Ti oxides with application to the deep lunar mantle. Earth Planet. Sci. Lett. 628, 118570.
Roy Choudhury, S., Dey, A., Mukherjee, S., Sengupta, S., Sanyal, S., Karmakar, S., Sengupta, P., 2023. Formation of aluminous clinopyroxene-ilmenite-spinel symplectic assemblage in a regionally metamorphosed calc-silicate granulite from the Chotanagpur Granite Gneiss Complex, East Indian shield. Lithos, 442-443, 107058.
Schmidt, M.W., Kraettli, G., 2022. Experimental crystallization of the lunar magma ocean, initial selenotherm and density stratification, and implications for crust formation, overturn and the bulk silicate Moon composition. J. Geophys. Res.: Planets 127 e2022JE007187.
Scholpp, J., Dygert, N., 2024. Experimental insights into the mineralogy and melt-rock reactions produced by lunar cumulate mantle overturn. Contrib. Mineral. Petrol. 179, 58.
Scholpp, J., Dygert, N., 2026. Trace element and isotopic evolution of the lunar interior during magma ocean solidification, cumulate overturn, and subsequent melting: insights into lunar melt sources. J. Geophys. Res.: Planets 131 e2024JE008865.
Shearer, C., Papike, J., 1999. Magmatic evolution of the Moon. Am. Mineral. 84, 1469–1494.
Shen, J., Zhang, Y., Wang, Z., Zuo, Z., Che, X., Li, W.-C., Wang, F., Li, S., Hu, Y., Hui, H., 2025. A pristine low-Ti cumulate source for Chang'e 5 basalts revealed by Sr-Nd-Hf isotopes. Geochem. Perspect. Lett. 33, 44–50.
Singletary, S., Grove, T., 2008. Origin of lunar high-titanium ultramafic glasses: a hybridized source? Earth Planet. Sci. Lett. 268, 182–189.
Snyder, G.A., Taylor, L.A., Neal, C.R., 1992. A chemical model for generating the sources of mare basalts: combined equilibrium and fractional crystallization of the lunar magmasphere. Geochim. Cosmochim. Acta 56, 3809–3823.
Springer, W., Seck, H.A., 1997. Partial fusion of basic granulites at 5 to 15 kbar: implications for the origin of TTG magmas. Contrib. Mineral. Petrol. 127, 30–45.
Su, B., Yuan, J., Chen, Y., Yang, W., Mitchell, R.N., Hui, H., Wang, H., Tian, H., Li, X.-H., Wu, F.-Y., 2022. Fusible mantle cumulates trigger young mare volcanism on the Cooling Moon. Sci Adv 8, eabn2103.
Sun, C.G., Graff, M., Liang, Y., 2017. Trace element partitioning between plagioclase and silicate melt: the importance of temperature and plagioclase composition, with implications for terrestrial and lunar magmatism. Geochim. Cosmochim. Acta 206, 273–295.
Taylor, G.J., Wieczorek, M.A., 2014. Lunar bulk chemical composition: a post-Gravity Recovery and Interior Laboratory reassessment. Philos. Trans. Royal Soc. A 372, 20130242.
Taylor, S.R., 1982. Planetary science: a lunar perspective. Lunar Planet. Inst. 502.
Tian, H.-C., Wang, H., Chen, Y., Yang, W., Zhou, Q., Zhang, C., Lin, H.-L., Huang, C., Wu, S.-T., Jia, L.-H., 2021. Non-KREEP origin for Chang'e-5 basalts in the Procellarum KREEP Terrane. Nature 600, 59–63.
Tsuno, K., Dasgupta, R., 2011. Melting phase relation of nominally anhydrous, carbonated pelitic-eclogite at 2.5–3.0 GPa and deep cycling of sedimentary carbon. Contrib. Mineral. Petrol. 161, 743–763.
Tsuno, K., Dasgupta, R., 2015. Fe–Ni–Cu–C–S phase relations at high pressures and temperatures–The role of sulfur in carbon storage and diamond stability at mid-to deep-upper mantle. Earth Planet. Sci. Lett. 412, 132–142.
Turner, G., 1971. 40Ar39Ar ages from the lunar maria. Earth Planet. Sci. Lett. 11, 169–191.
van Kan Parker, M., Sanloup, C., Sator, N., Guillot, B., Tronche, E.J., Perrillat, J.-P., Mezouar, M., Rai, N., van Westrenen, W., 2012. Neutral buoyancy of titanium-rich melts in the deep lunar interior. Nat. Geosci. 5, 186–189.
Wagner, T., Grove, T., 1997. Experimental constraints on the origin of lunar high-Ti ultramafic glasses. Geochim. Cosmochim. Acta 61, 1315–1327.
Walker, D., Kirkpatrick, R., Longhi, J., Hays, J., 1976. Crystallization history of lunar picritic basalt sample 12002: phase-equilibria and cooling-rate studies. Geol Soc Am Bull 87, 646.
Wang, C., Xu, Y.-G., Zhang, L., Chen, Z., Xia, X., Lin, M., Guo, F., 2024a. A shallow (<100 km) ilmenite-bearing pyroxenitic source for young lunar volcanism. Earth Planet. Sci. Lett. 639, 118770.
Wang, Z., Li, Y., Zhang, W., He, Q., Pan, F., Hu, Z., Zong, K., Feng, Y., Becker, H., Day, J. M.D., Song, W., Hui, H., Moynier, F., Jiang, Y., Zhang, X., She, Z., Wu, X., Xiao, L., Wang, L., 2024b. Sulfide compositions of young Chang'e-5 basalts and implications for sulfur isotopes in lunar basalt sources. Geochim. Cosmochim. Acta 368, 168–184.
Wang, Z., Zong, K., Li, Y., Li, J., He, Q., Zou, Z., Becker, H., Moynier, F., Day, J.M.D., Zhang, W., Qian, Y., Xiao, L., Hu, Z., She, Z., Hui, H., Wu, X., Liu, Y., 2024c. Young KREEP-like mare volcanism from Oceanus Procellarum. Geochim. Cosmochim. Acta 373, 17–34.
Warren, P.H., 1989. KREEP: major-element diversity, trace-element uniformity (almost), Workshop on Moon in Transition: apollo 14. KREEP, Evolved Lunar Rocks 149–153.
Warren, P.H., 2005. New" lunar meteorites: implications for composition of the global lunar surface, lunar crust, and the bulk Moon. Meteorit Planet Sci. 40, 477–506.
Warren, P.H., Wasson, J.T., 1979. The origin of KREEP. Rev. Geophys. 17, 73–88.
Weber, R.C., Lin, P.-Y., Garnero, E.J., Williams, Q., Lognonné, P., 2011. Seismic detection of the lunar core. science 331, 309–312.
Wood, M.C., Gréaux, S., Kono, Y., Kakizawa, S., Ishikawa, Y., Inoué, S., Kuwahara, H., Higo, Y., Tsujino, N., Irifune, T., 2024. Sound velocities in lunar mantle aggregates at simultaneous high pressures and temperatures: implications for the presence of garnet in the deep lunar interior. Earth Planet. Sci. Lett. 641, 118792.
Wu, F.-Y., Li, Q.-L., Chen, Y., Hu, S., Yue, Z.-Y., Zhou, Q., Wang, H., Yang, W., Tian, H.-C., Zhang, C., Li, J.-H., Li, L.-X., Hui, H.-J., Li, C.-L., Lin, Y.-T., Li, X.-H., Delano, J.W., 2024. Lunar evolution in light of the Chang'e-5 returned samples. Annu. Rev. Earth Planet Sci. 52, 159–194 null.
Yang, W., Chen, Y., Wang, H., Tian, H.-C., Hui, H., Xiao, Z., Wu, S.-T., Zhang, D., Zhou, Q., Ma, H.-X., Zhang, C., Hu, S., Li, Q.-L., Lin, Y., Li, X.-H., Wu, F.-Y., 2022. Geochemistry of impact glasses in the Chang'e-5 regolith: constraints on impact melting and the petrogenesis of local basalt. Geochim. Cosmochim. Acta 335, 183–196.
Zong, K., Wang, Z., Li, J., He, Q., Li, Y., Becker, H., Zhang, W., Hu, Z., He, T., Cao, K., 2022. Bulk compositions of the Chang'E-5 lunar soil: insights into chemical homogeneity, exotic addition, and origin of landing site basalts. Geochim. Cosmochim. Acta 335, 284–296.